Effects of temperature and salinity on fouling in hypersaline seawater

Bing Ni, Shengqiang Shen*, Xiaohua Liu, Shi Chen

Liaoning Key Laboratory of Desalination, School of Energy and Power Engineering, Dalian University of Technology, Dalian 116024, China, emails: zzbshen@dlut.edu.cn (S.Q. Shen), 378459679@qq.com (B. Ni), 593494899@qq.com (X.H. Liu), 592068882@qq.com (S. Chen)

ABSTRACT

Fouling is an essential obstacle in seawater treatment. This paper studies the effects of temperature and salinity on fouling characteristics, in particular to reveal scaling crystals that affect the deposition amount with the technique of static deposition in hypersaline seawater. The results show that the deposition amount on the titanium tube surface decreases with increasing salinity at a temperature of 80°C, achieving the highest value at the salinity of 8%. In comparison with that at 80°C, the change trend in deposition amount is different at the temperature of 90°C achieving the largest value at the salinity of 12%. The major composition on the metallic surface is $Mg(OH)_2$ at diverse working conditions. Moreover, $CaSO_4$ and $CaCO_3$ crystals are suspended in the beaker, while bulk crystals eventually deposit at the bottom of the beaker.

Keywords: Salinity; Temperature; Fouling; Hypersaline seawater; Desalination

1. Introduction

The pollution of hypersaline seawater is becoming increasingly serious in seawater desalination and treatment of high-salt wastewater. If this part of seawater is discharged, the energy of concentrated seawater cannot be effectively used, and the environment can be polluted. At present, the salt can be recycled and extracted in the solution. The application of evaporation and cooling extraction is extensive [1]. Fouling is deposited on the heat transfer surface during the process of seawater treatment. The fouling not only decreases heat transfer performance but also increases flow resistance. Therefore, the study on restraining fouling has become a hotspot.

Scholars summarize the methods of inhibiting crystallization of $CaCO_3$ [2] and $CaSO_4$ [3] and other crystals [4]. The methods of adding crystal seeds can reduce the fouling adsorption capacity on the heat transfer surface [5], and using crystal seeds with the same composition as fouling has better effect [6]. Addition of the crystal seeds reduces the supersaturation of the solution and decreases the deposition

amount. Therefore, Linnikov [7] studied the effects of crystal seeds concentration on crystallization. Equations describing these processes are derived. The result indicated that theoretical equation is consistent with the literature data. Omar et al. [8], and Al-Ghamdi and Omar [9] used Ryznar Stability Index as a characterization index with $CaCO_3$ as crystal seeds. They identified that the scaling tendency of the fouling slows down after adding crystal seeds, and the stability index increases. Omar et al. [10] adopted a method of adding crystal seeds to reducing the scaling tendency of $CaCO_3$ in a seeded batch crystallizer. The experimental results indicated that the growth rate of $CaCO_3$ increases with the upgrade of temperature and the seeds ratio of input (above 1 g L^{-1}).

Numerous studies have summarized the effect factors of fouling deposition characteristics, such as flow rate [11,12], temperature [13], water quality parameters, concentration, etc. Pääkkönen et al. [14] concluded that the scale-formation rate of $CaCO_3$ on a heated wall decreases with the increase of flow velocity at high-wall temperature. The solution with high pH value can avoid acidic corrosion on the heat exchanger. But free hydrogen ions are reduced,

---

* Corresponding author.

and alkaline salts are deposited easily after increasing pH value. Therefore, Hofling et al. [15] performed the effect experiments of pH value on fouling deposition using mixed aqueous solution of $CaCO_3$ concentration of 0.005 mol L^{-1} and $CaSO_4$ concentration of 0.03 mol L^{-1}. The experimental results showed that in the scale layers, only $CaSO_4$ is detected at the pH value of 6.0, and $CaCO_3$ is detected after the pH value reached 7.0.

Peyghambarzadeh and Bahrami [16] argued that concentration is more important than other effect factors on the fouling. Shen et al. [17] studied the effect of concentration on the scaling process of $CaCO_3$. They derived that heterogeneous nucleation rate and growth rate of crystals are enhanced with the increase of $CaCO_3$ concentration on the surface of heat exchanger. In the study of seawater, Krömer et al. [18] and Stärk et al. [19] detected mixed fouling in a multi-effect evaporator by scanning electron microscope (SEM) and energy dispersive X-ray detector. The experimental results indicated that $CaCO_3$ precipitates on the scale layers of $Mg(OH)_2$. The deposition amount of $CaCO_3$ increases with the decrease of Mg^{2+} concentration in the solution. Yang et al. [20] performed experiments to study fouling formation in a heat exchanger using seawater with Mg^{2+} concentration of 1,272 mg L^{-1} and Al^{3+} concentration of 164 mg L^{-1}. The results indicated that elevated temperature and increased salinity can aggravate the fouling deposition. The concentration of Al^{3+} is higher than normal seawater. Therefore, in addition to $Mg(OH)_2$, $Al(OH)_3$ is deposited on the surface of heat transfer. Rawajfeh [21] established a mathematical model for calculating deposition of $CaCO_3$ on the heat transfer surface. The salinity range was 2.5% to 6.7%. The simulation results showed that $CaCO_3$ deposition rates increase with increasing salinity. Wildebrand et al. [22] studied the scaling process in the horizontal tube surface of a multi-effect evaporator. The salinity range was 3.5% to 6.5%. The experimental results demonstrated that the fouling deposition rate increases with the increase of temperature and salinity. Therefore, the deposition of fouling increases with increasing salinity at a certain range in seawater.

Discussion about fouling characteristics of hypersaline seawater has seldom been published at high-temperature conditions. In addition, most researchers neglect the effect of precipitated particles after the increase of supersaturation degree. They focus on the method of adding crystal seeds. This paper is to study the fouling characteristics at high-temperature and high-salt conditions with the technique of static deposition. The results are significant to alleviate fouling deposition treatment of high-salt seawater.

2. Materials and methods

In this experiment, natural seawater (c = 3.5%) is used. The ionic concentration is analyzed using an ion chromatography analyzer (DIONEX ICS-5000). Ions are detected in a weak acidic environment. Therefore, HCO_3^- is detected by titration. The ionic composition and ionic concentration of seawater are given in Table 1. The seawater is obtained from the Bohai Gulf that is rich in magnesium ore. Therefore, in addition to Na^+ and Cl^-, Mg^{2+} concentration is higher. Seawater of diverse salinity is obtained by isothermal evaporation.

Table 1
Main ionic concentration of experimental seawater (mol L^{-1})

Ion	Concentration	Ion	Concentration
Na^+	0.490	SO_4^{2-}	0.030
K^+	0.012	HCO_3^-	0.002
Ca^{2+}	0.011	Br^-	0.001
Mg^{2+}	0.066	Cl^-	0.550

Fig. 1. Schematic of experimental system.

Fig. 1 depicts a diagram of the experimental system. The concentrated seawater and titanium tube are put into beakers. The beakers are placed on the thermostat heater. The thermostat heater is adjusted to control the liquid temperature. The insulation material is wrapped outside the beakers to reduce heat dissipation loss.

The titanium tube with a diameter of 25 mm and a length of 20 mm is used in the experiment. The titanium tube and 20.0 mL seawater are both placed in the beaker. The axis of the titanium tube is perpendicular to the bottom of the beaker. The titanium tube is removed and placed into deionized water to dissolve the soluble salt every 10 h. Following this, the titanium tubes are weighed by a precision balance. Tweezers are used to pick up the titanium tube to prevent the fouling from falling off. Three samples are selected for each group to obtain an average value. Deionized water is added to the beakers every 10 h. After the experiment, the crystals in the beakers are filtered using filter paper. Finally, the morphology and composition of the fouling and crystals are analyzed by SEM and energy dispersive X-ray (EDX) after 60 h.

Solubility of insoluble salt may alter with salinity in the strong electrolyte solutions. To judge whether crystals are precipitated, the solubility product is calculated using the Pitzer method. Ionic product is calculated using ionic concentration of experimental seawater. The result of precipitation is verified using the difference between ion product Q_i and solubility product K_{sp}.

Pitzer [23,24] derived the Pitzer model of strong electrolyte solutions. In this paper, activity coefficients of each ion are calculated according to the Pitzer model in the seawater, and then the solubility product is calculated by Eq. (1).

$$K_{sp} = \frac{K_{sp}^{\Theta}}{\gamma_{M^+} \cdot \gamma_{A^-}}$$
(1)

where K_{sp}^{Θ} and K_{sp} are the activity product and solubility product, respectively. γ_{M^+} and γ_{A^-} are the activity coefficients of the electrolyte anion and cation, respectively.

Figs. 2–4 represent the calculated results of the solubility product. The ionic products are given in Tables 2–4.

The judging method of crystals precipitation and dissolution is as follows:

When Q_i is greater than K_{sp}, the hard-soluble electrolyte solution is oversaturated. Crystal is precipitated until the solution reaches a new balance; When Q_i is equal to K_s, the hard-soluble electrolyte solution is saturated. Crystals are not precipitated; When Q_i is less than K_{sp}, the hard-soluble electrolyte solution is unsaturated. Crystals are not precipitated.

The difference between ionic product and solubility product are defined as the supersaturation degree of electrolyte.
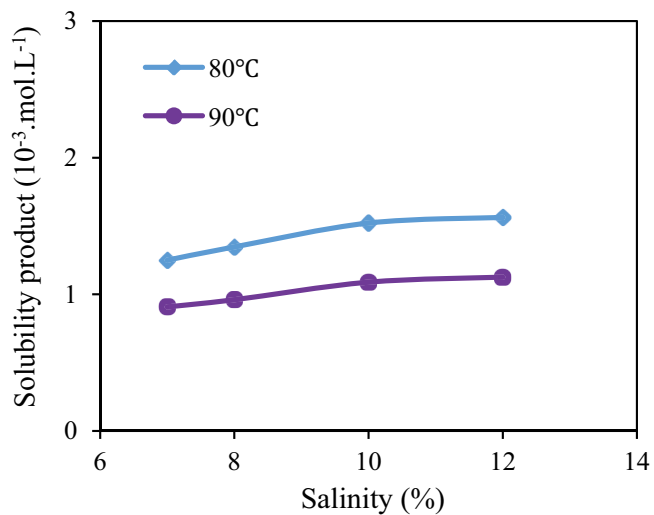
Fig. 2. Solubility product of CaSO$_4$ in seawater at various temperature and salinity.
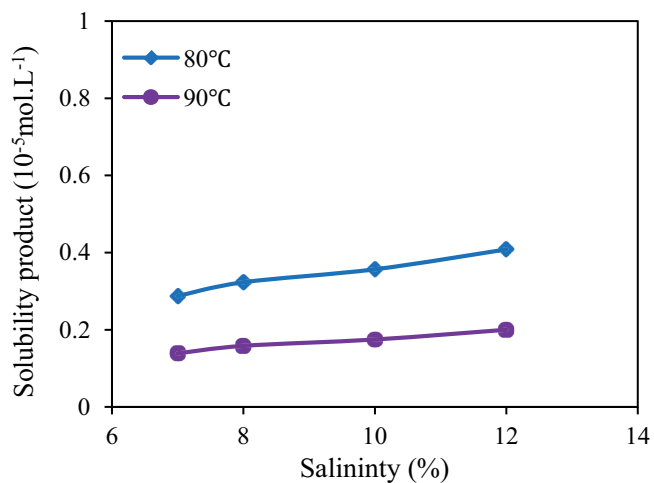
Fig. 3. Solubility product of CaCO$_3$ in seawater at various temperature and salinity.
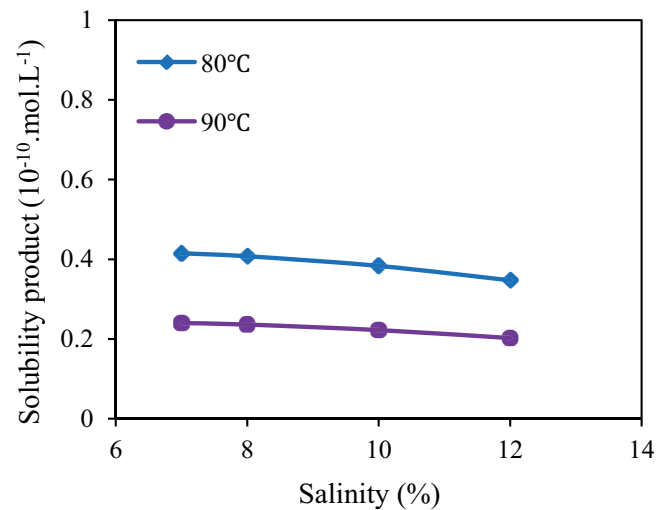
Fig. 4. Solubility product of Mg(OH)$_2$ in seawater at various temperature and salinity.

Table 2
Ionic product of CaSO$_4$ at diverse temperature and salinity ($Q_i \times 10^3$)

Temperature	Salinity			
	7%	8%	10%	12%
80°C	0.863	1.127	1.608	2.359
90°C	0.789	1.031	1.277	1.97

Table 3
Ionic product of CaCO$_3$ at diverse temperature and salinity ($Q_i \times 10^5$)

Temperature	Salinity			
	7%	8%	10%	12%
80°C	4.62	5.37	7.14	9.96
90°C	4.119	4.77	5.89	7.33

Table 4
Ionic product of Mg(OH)$_2$ at diverse temperature and salinity ($Q_i \times 10^5$)

Temperature	Salinity			
	7%	8%	10%	12%
80°C	0.372	0.432	0.520	0.644
90°C	0.291	0.338	0.416	0.548

3. Results and discussion

3.1. Fouling deposition on the surface of a titanium tube

To study fouling deposition characteristics of high salinity seawater, mass increment of fouling per unit area is obtained using the weigh method at diverse temperatures. The temperature of experimental seawater is 70°C, 80°C and 90°C, respectively. The salinity of experimental seawater is 7%, 8%, 10% and 12%, respectively. The results are presented in Figs. 5–7.

The data in Fig. 5 show that after 10 h, the mass increment is negative at the salinity of 7% and 8%. Because the fouling precipitate is less at lower salinity, and impurities are attached on the surface of the titanium tube. The impurities are dissolved in the solution after being heated. The mass increment of 10% is zero. This is because the dissolved-impurities mass and deposited-fouling mass are balanced on the titanium tube surface.

In Fig. 6, the mass increment of fouling stabilizes after 30 h at the temperature of 80°C. An unanticipated finding is that the mass increment of fouling reduces with increasing
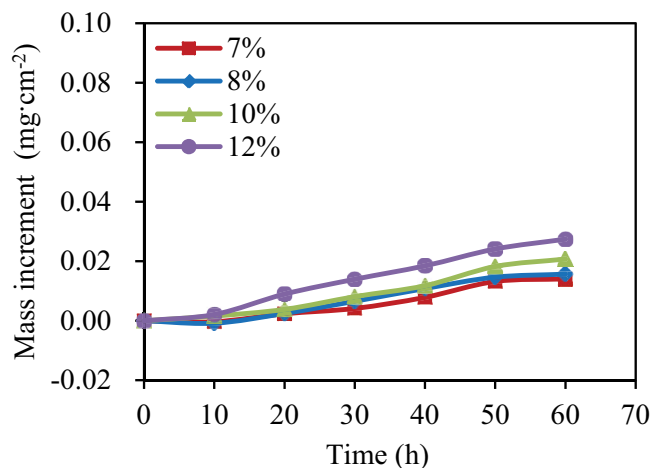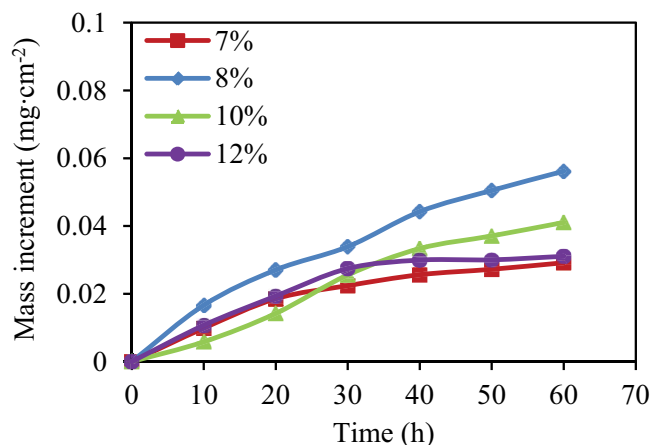
salinity. The curves in Fig. 6 indicate that the mass increments of fouling at the salinity of 10% and 12% are less than that at the salinity of 8%. The mass increment of fouling reaches the smallest value at the salinity of 7%. The supersaturation degree of $CaSO_4$ is -0.387×10^{-3}, -0.22×10^{-3}, 0.088×10^{-3} and 0.799×10^{-3} with seawater salinity of 7%/8%/10%/12%, respectively. Therefore, $CaSO_4$ is precipitated when salinity is greater than 8%. Similarly, $CaCO_3$ and $Mg(OH)_2$ reach supersaturation at different conditions. The deposition amounts of $CaCO_3$ and $Mg(OH)_2$ are minor and $CaSO_4$ is not precipitated at low salinity. Therefore, the deposition of fouling is the least at the salinity of 7%. With the increase of salinity, the number of particles in the beaker increases, which provide sites of secondary nucleation. Therefore, the mass increment of fouling decreases on the titanium tube surface.

What is noteworthy in Fig. 7 is that the mass increment of fouling at the salinity of 10% is less than at 8%. The fouling mass increment with 7% salinity is the least and that with 12% salinity is maximal. The data in Fig. 7 are compared with the data in Figs. 5 and 6, showing that with the temperature rising, the mass increment of fouling significantly increases. The supersaturation degree of $CaSO_4$ is -0.111×10^{-3}, 0.07×10^{-3}, 0.188×10^{-3} and 0.845×10^{-3} with the seawater salinity of 7%/8%/10%/12%, respectively, at the temperature of 90°C. Therefore, $CaSO_4$ is precipitated when salinity is above 7%. The supersaturated states of $CaCO_3$ and $Mg(OH)_2$ at the temperature of 90°C are the same as that at the temperature of 80°C. The supersaturation of electrolyte increases at the salinity of 12% than that at the salinity of 10%. Therefore, the precipitated crystals quantity increases. Some crystals are attached to the titanium tube surface in the form of heterogeneous nucleation. Currently, the primary nucleation rate of crystal is accelerated. The crystals are attached on the titanium tube surface. Therefore, the deposition amount of the fouling is maximal at the salinity of 12%.

Fig. 5. Mass increment of fouling per unit area as a function of time for various salinity at $T = 70°C$.

3.2. Fouling composition and microstructure

The crystals are suspended in the solution by secondary nucleation, and these crystals are not deposited on the surface of the titanium tube. Only using the judging method is

Fig. 6. Mass increment of fouling per unit area as a function of time for various salinity at $T = 80°C$.
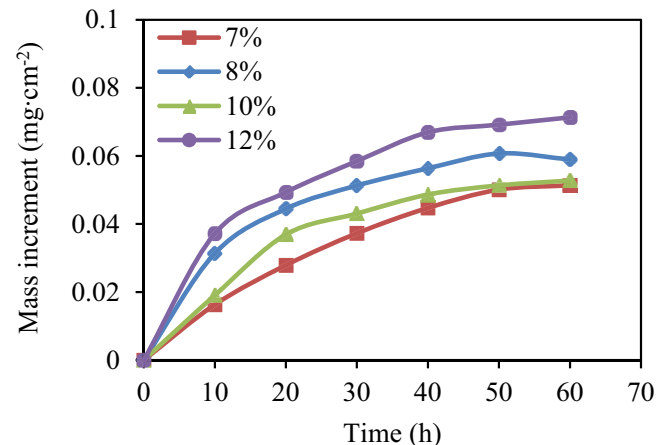
Fig. 7. Mass increment of fouling per unit area as a function of time for various salinity at $T = 90°C$.

imprecise to determine whether the crystals are deposited on the titanium tube surface. Therefore, EDX detector and SEM are used to analyze the precipitated crystals. In this paper, the seawater temperature is 90°C as an example. The seawater salinity is 7%, 8%, 10% and 12%, respectively.

The main forms of calcium sulfate are $CaSO_4 \cdot 2H_2O$, $CaSO_4 \cdot 1/2H_2O$ and anhydrous $CaSO_4 \cdot 2H_2O$ and $CaSO_4 \cdot 1/2H_2O$ are crystals of monoclinic system. Anhydrous $CaSO_4$ is crystal of orthorhombic system. The main forms of calcium carbonate are spherical aragonite, calcite and aragonite. Different forms of calcium carbonate are formed from amorphous calcium carbonate. Spherical aragonite and aragonite are mild scale and easy to remove. Calcite is the most stable and difficult to remove.

3.2.1. Fouling composition and micro-topography at the salinity of 7%

Fig. 8a presents the SEM images of the deposition on the surface of titanium tube with 10,000-fold magnification at the salinity of 7%. Fig. 8b provides the SEM images of the deposition in the beakers with 5,000-fold magnification at the salinity of 7%. Table 5 presents the EDX analysis results of fouling composition and percentage in Fig. 8
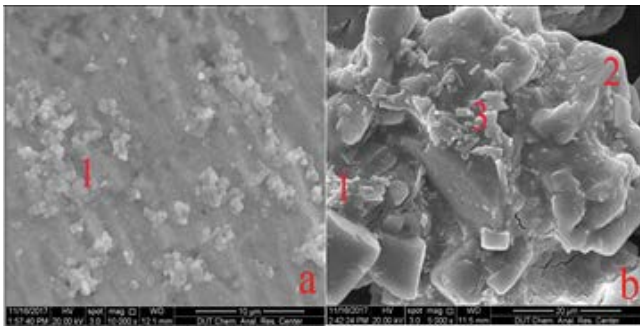
Fig. 8. SEM images showing the titanium tube surface and crystals in the beaker at the salinity of 7% (a) fouling of the titanium tube surface and (b) crystals precipitation at the bottom of beaker. 1 – $Mg(OH)_2$, 2 – NaCl, 3 – aragonite $CaCO_3$.

Table 5
Fouling components of the titanium tube surface and beaker bottom (%)

Titanium tube surface (a)		Crystals in beaker (b)	
Element	Weight percentage	Element	Weight percentage
O	39.18	O	32.98
Na	0.56	Na	16.56
Cl	0.36	Cl	31.37
Mg	2.93	Mg	9.42
S	0.06	S	0.14
Si	1.44	Si	1.34
Ti	48.78	Ca	2.95
C	6.68	C	5.24
Totals	100.00	Totals	100.00

The titanium tube is selected in the experiment. Therefore, the content of Ti is more than that of others elements in the EDX analysis of the sample. A large amount of hydroxides is adhered on the surface of the titanium tube. Therefore, the content of O is higher.

According to the analysis in Fig. 8a and Table 5a, the crystals attached on the surface of titanium tube are flaky $Mg(OH)_2$. $Mg(OH)_2$ crystals affect the deposition of $CaCO_3$. $CaSO_4$ is unsaturated at the salinity of 7%. Therefore, $CaSO_4$ is not deposited on the surface of titanium tube. Table 5b shows that the scale-forming elements are Mg and Ca; the weight percentages of Na and Cl are 16.56% and 31.37%, respectively. NaCl crystals are precipitated when filtered crystals are dried. Fig. 8b presents that the minor crystals attach to the surface of square NaCl crystals. Crystals of adhesion are aragonite $CaCO_3$, flaky $Mg(OH)_2$ and amorphous crystals. The edge of $CaCO_3$ crystals is glazed. This result is due to the edge of the crystals came in contact with the solution and dissolve easily. The crystals in the beaker contain 0.14% of S and 2.95% of Ca. However, in Fig. 8b, the crystal in $CaSO_4$ form was not observed. There are two possible explanations for this result. One might be that amorphous crystal containing S and Ca is precipitated. Another is that a spot of $CaSO_4$ is precipitated when the filtered crystals are dried.

3.2.2. Fouling composition and micro-topography at the salinity of 8%

Fig. 9a presents the SEM images of the deposition on the surface of titanium tube with 10,000-fold magnification at the salinity of 8%. Fig. 9b provides the SEM images of the deposition in the beakers with 5,000-fold magnification at the salinity of 8%. The EDX analysis results of Fig. 9 are shown in Table 6.

According to the analysis in Fig. 9a and Table 6a, the crystals attached on the surface of titanium tube are still flaky $Mg(OH)_2$. Aragonite $CaCO_3$, flaky $Mg(OH)_2$, NaCl and amorphous crystals are precipitated at the bottom of beaker. Mg^{2+} is significant to promote dissolution of $CaSO_4$ [25]. This is because Mg^{2+} and SO_4^{2-} in the solution generate magnesium sulfate ion pairs to alter the dissolution equilibrium of $CaSO_4$ [26]. Magnesium sulfate ion pair increases with increasing concentration of Mg^{2+}, and these ion pairs promote the dissolution of $CaSO_4$. The solubility of $CaSO_4$
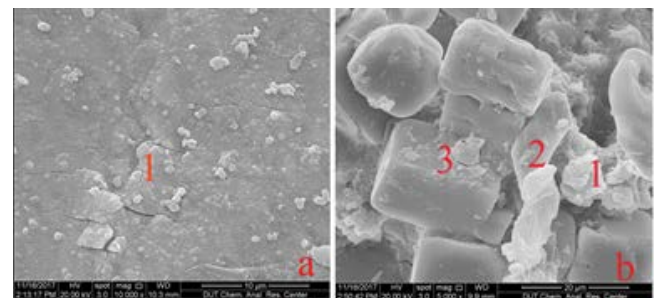
Fig. 9. SEM images showing the titanium tube surface and crystals in the beaker at the salinity of 8% (a) fouling of the titanium tube surface and (b) crystals precipitation at the bottom of beaker. 1 – $Mg(OH)_2$, 2 – aragonite $CaCO_3$, 3 – NaCl.

in seawater is higher than that in water. The supersaturation degree of $CaSO_4$ is 0.07×10^{-3} at the salinity of 8%. In Fig. 9, the crystals in $CaSO_4$ form are still not observed. This result indicates that $CaSO_4$ is not precipitated in large quantities at the salinity of 8%. Currently, mass increment of fouling on the surface of titanium tube is not affected by $CaSO_4$.

Table 6
Fouling components of the titanium tube surface and beaker bottom (%)

Titanium tube surface (a)		Crystals in beaker (b)	
Element	Weight percentage	Element	Weight percentage
C	6.54	C	25.74
O	36.71	O	14.96
Ca	0.03	Ca	0.34
Ti	52.72	Cl	34.77
Si	0.98	Na	19.92
Mg	2.80	Mg	3.64
S	0.03	S	0.15
Others	0.2	Others	0.48
Totals	100.00	Totals	100.00

3.2.3. Fouling composition and micro-topography at the salinity of 10%

Fig. 10a presents the SEM images of the deposition on the surface of titanium tube with 10,000-fold magnification at the salinity of 10%. Fig. 10b provides the SEM images of the deposition in the beakers with 3,000-fold magnification at the salinity of 10%. The results obtained from the EDX analysis of Fig. 10 are presented in Table 7. Table 7b is the crystal analysis of the $CaSO_4$ surface in Fig. 10b.

According to the analysis of Fig. 10a and Table 7a, only flaky $Mg(OH)_2$ cover the surface of titanium tube. The supersaturation degree of $CaSO_4$ is 0.188×10^{-3} at the salinity of 10%. Table 7b provides that the weight percentages of Ca and S are 15.35% and 14.22%, respectively. Fig. 10b presents that the minor crystals attach to the surface of square $CaSO_4$ and NaCl crystals. The adhesion crystals are aragonite $CaCO_3$, flaky $Mg(OH)_2$ and amorphous crystals. This result indicates that $CaSO_4$ is precipitated when the supersaturation degree is 0.188×10^{-3}. In Fig. 10b, the crystals of tetrahedron columnar are orthorhombic system. Therefore, it can be judged that tetrahedron columnar crystals are anhydrous $CaSO_4$. $CaSO_4$ are suspended by homogeneous nucleation in solution at the salinity of 10%. These particles provide the growth sites of secondary nucleation for $CaSO_4$ crystals of continuous precipitation and inhibit the precipitation of crystals on the titanium tube surface.

Fig. 10. SEM images showing the titanium surface and crystals in the beaker at the salinity of 10% (a) fouling of the titanium tube surface and (b) crystals precipitation at the bottom of beaker. 1 – $Mg(OH)_2$, 2 – $CaSO_4$, 3 – aragonite $CaCO_3$, 4 – NaCl.
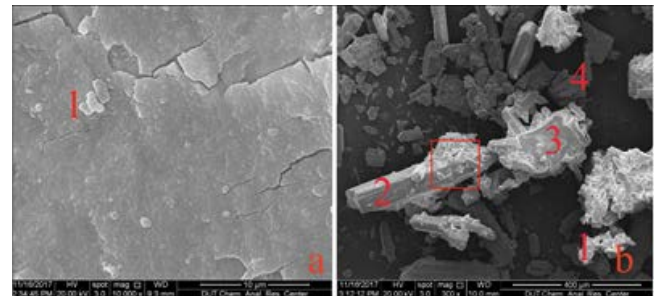
Fig. 11. SEM images showing the titanium tube surface and crystals in the beaker at the salinity of 12% (a) fouling of the titanium tube surface and (b) crystals precipitation at the bottom of beaker. 1 – $Mg(OH)_2$, 2 – $CaSO_4$, 3 – NaCl, 4 – calcite $CaCO_3$.

Table 7
Fouling components of the titanium tube surface and beaker bottom (%)

Titanium tube surface (a)		Crystals in beaker (b)			
Element	Weight percentage	Element	Weight percentage	Element	Weight percentage
O	33.47	O	19.85	S	14.22
Ti	53.60	Na	5.96	C	19.85
Mg	3.87	Cl	8.71	K	0.87
Si	1.97	Ca	15.35		
C	7.09	Mg	1.89		
Totals	100.00			Totals	100.00

Table 8
Fouling components of the titanium tube surface and beaker bottom (%)

Titanium tube surface (a)		Crystals in beaker (b)	
Element	Weight percentage	Element	Weight percentage
C	5.45	C	21.15
O	33.49	O	38.45
Mg	4.83	Mg	3.13
Ca	0.06	Ca	10.31
Si	2.26	S	10.18
Fe	0.28	Na	4.73
Ti	53.62	Cl	10.12
		Others	1.93
Totals	100.00	Totals	100.00

3.2.4. Fouling composition and micro-topography at the salinity of 12%

Fig. 11a presents the SEM images of the deposition on the surface of titanium tube with 10,000-fold magnification at the salinity of 12%. Fig. 11b provides the SEM images of the deposition in the beakers with 300-fold magnification at the salinity of 12%. Table 8a presents the EDX analysis results of fouling composition and percentage in Fig. 8a. Table 8b is the crystal analysis of the $CaSO_4$ surface in Fig. 11b.

The titanium tube is cooled before weighing, and the fouling crack and shed under the action of thermal expansion and contraction as shown in Fig. 11a. The $CaSO_4$ is not precipitated on the surface of a titanium tube. This result is due to higher Mg^{2+} concentration affects the crystallization and adsorption of $CaSO_4$ crystals on the titanium tube surface. $CaSO_4$ crystals are suspended in solution by secondary nucleation. Inside the filtered crystals, $Mg(OH)_2$, aragonite $CaCO_3$ and amorphous crystals attach on the surface of $CaSO_4$ crystals.

$CaCO_3$ is not precipitated on the titanium tube surface at diverse salinities. This is because that $CaCO_3$ is suspended in the solution by secondary nucleation. Meanwhile, the surface energy of titanium tube is lower than that of other metals. $CaCO_3$ sheds easily from the surface of a titanium tube. In conclusion, the mass increment of fouling on a titanium tube surface is not affected by $CaCO_3$ and $CaSO_4$.

4. Conclusions

The effects of scale formation on a titanium tube surface are studied using concentrated seawater. This paper shows that the temperature and salinity of seawater affect the deposited amount of fouling. The results of the study are helpful to the treatment of high salinity water.

The main component of fouling on a titanium tube surface is $Mg(OH)_2$ at experimental conditions. The mass increment of fouling per unit area is affected by the deposition characteristics of $Mg(OH)_2$ crystals at diverse salinities. The mass increment of fouling increases with the increase of salinity at the temperature of 70°C; Increasing the seawater salinity to 8%, the mass increment of fouling reduces with the increase of salinity at the temperature of 80°C; Increasing the temperature to 90°C, the mass increment of fouling at the salinity of 10% is less than that at the salinity of 8%. Mass increment of fouling reaches the maximum value at the salinity of 12%.

$CaSO_4$ crystals are not deposited on the surface of a titanium tube at experimental conditions. $CaSO_4$ is not oversaturated when the salinity is below 8%; $CaSO_4$ crystals deposited on the existing particles and are suspended in the solution after reaching supersaturation. Eventually, the crystals precipitated at the bottom of the beaker due to the action of gravity.

References

[1] D.H. Kim, A review of desalting process techniques and economic analysis of the recovery of salts from retentates, Desalination, 270 (2011) 1–8.
[2] A.G. Pervov, Precipitation of calcium carbonate in reverse osmosis retentate flow by means of seeded techniques — a tool to increase recovery, Desalination, 368 (2015) 140–151.
[3] H. Wang, D. Wang, Z. Li, G.P. Demopoulos, Solubility and scale prevention of gypsum in transportation pipes of well brine with salinities up to 5 M at temperature range of 278–298 K, Desal. Wat. Treat., 22 (2010) 78–86.
[4] K. Moriyama, T. Kojima, Y. Minawa, S. Matsumoto, K. Nakamachi, Development of artificial seed crystal for crystallization of calcium phosphate, Environ. Technol., 22 (2001) 1245–1252.
[5] J. Liu, J.J. Yuan, Calcium sulfate scaling and its advances in application of control techniques, Tianjin Chem. Ind., 24 (2010) 10–14.
[6] H.G. Dong, J. Ding, Z.Q. Shen, Experimental research for fouling-proof by introducing seeding crystal, Chem. Eng. (China), 27 (1999) 16–19.
[7] O.D. Linnikov, About seed concentration for prevention of scale, Desalination, 157 (2003) 235–240.
[8] W. Omar, J. Chen, J. Ulrich, Reduction of seawater scale forming potential using the fluidized bed crystallization technology, Desalination, 250 (2010) 95–100.
[9] A. Al-Ghamdi, W. Omar, Application of pellet softening (PS) as a scale prevention method in seawater desalination plants, Desal. Wat. Treat., 51 (2013) 5509–5515.
[10] W. Omar, J. Chen, J. Ulrich, Application of seeded batch crystallization methods for reduction of the scaling tendency of seawater-A study of growth kinetics of calcium carbonate in seawater, Crystal Res. Technol., 44 (2010) 469–476.
[11] B.O. Hasan, G.J. Nathan, P.J. Ashman, R.A. Craig, R.M. Kelso, The use of turbulence generators to mitigate crystallization fouling under cross flow conditions, Desalination, 288 (2012) 108–117.
[12] B.O. Hasan, G.J. Nathan, P.J. Ashman, R.A. Craig, R.M. Kelso, The effects of temperature and hydrodynamics on the crystallization fouling under cross flow conditions, Appl. Thermal Eng., 36 (2012) 210–218.
[13] A.E. Al-Rawajfeh, S. Ihm, H. Varshney, A.N. Mabrouk, Scale formation model for high top brine temperature multi-stage flash (MSF) desalination plants, Desalination, 350 (2014) 53–60.
[14] T.M. Pääkkönen, M. Riihimäki, C.J. Simonson, E. Muurinen, R.L. Keisk, Crystallization fouling of $CaCO_3$-Analysis of

experimental thermal resistance and its uncertainty, Int. J. Heat Mass Transfer, 55 (2012) 6927–6937.

[15] V. Hofling, W. Augustin, M. Bohnet, Crystallization fouling of the aqueous two-component system $CaSO_4$/$CaCO_3$ fouling of salt mixtures, Int. J. Transport Phenom., 6 (2004) 99–110.

[16] S.M. Peyghambarzadeh, N. Bahrami, Statistical analysis of calcium sulfate scaling under boiling heat transfer, Appl. Thermal Eng., 53 (2013) 108–113.

[17] J. Shen, H. Zhang, P. Zhao, Characteristics of the initial stage of $CaCO_3$ crystallization fouling on two kinds of oblique fin tube, J. Univ. Shanghai Sci. Technol., 36 (2014) 443–448.

[18] K. Krömer, S. Will, K. Loisel, S. Nied, J. Detering, A. Kempter, H. Glade, Scale formation and mitigation of mixed salts in horizontal tube falling film evaporators for seawater desalination, Heat Transfer Eng., 36 (2014) 750–762.

[19] A. Stärk, K. Loisel, K. Odiot, A. Feßenbecker, A. Kempter, S. Nied, H. Glade, Wetting behaviour of different tube materials and its influence on scale formation in multiple-effect distillers, Desal. Wat. Treat., 55 (2015) 2502–2514.

[20] D. Yang, J. Liu, E. Xiaoxue, J. Linlin, Model for seawater fouling and effects of temperature, flow velocity and surface free energy on seawater fouling, Chin. J. Chem. Eng., 24 (2016) 658–664.

[21] A. E. Al-Rawajfeh, Modeling of alkaline scale formation in falling film horizontal-tube multiple-effect distillers, Desalination, 205 (2007) 124–139.

[22] C. Wildebrand, H. Glade, S. Will, M. Essig, J. Rieger, K. Büchner, G. Brodt, Effects of process parameters and anti-scalants on scale formation in horizontal tube falling film evaporators, Desalination, 204 (2007) 448–463.

[23] M. Whitfield, The extension of chemical models for sea water to include trace components at 25°C and 1 atm pressure, Geochim. Cosmochim. Acta, 39 (1975) 1545–1557.

[24] M. Whitfield, A chemical model for the major electrolyte component of seawater based on the Brønsted-Guggenheim hypothesis, Marine Chem., 1 (1973) 251–266.

[25] H. Wei, The conversion, modification and the solubility study of flue gas desulfurization gypsum at atmospheric pressure, Wuhan University of Science and Technology, China, 2009.

[26] T.H. Liu, D. Yan, F. Yang, C. Peng, S. Hao, Z.Y. Zheng, R. Liu, Influence of Al^{3+}, Na^+ and Mg^{2+} on crystallization of calcium sulfate dihydrate, J. Chem. Ind. Eng., 67 (2016) 296–301.